Rowan University

Rowan Digital Works

Faculty Scholarship for the College of Science & Mathematics

College of Science & Mathematics

8-20-2020

In Situ Electric-Field Study of Surface Effects in Domain Engineered Pb(In1/2Nb1/2)O3-Pb(Mg1/3Nb2/3)O3-PbTiO3 Relaxor Crystals by Grazing Incidence Diffraction

Markys G. Cain

Margo Staruch

Paul Thompson

Christopher Lucas

Didier Wermeille

See next page for additional authors

Follow this and additional works at: https://rdw.rowan.edu/csm_facpub

 Part of the Materials Science and Engineering Commons, and the Physics Commons

Recommended Citation

Cain, Markys G.; Staruch, Margo; Thompson, Paul; Lucas, Christopher; Wermeille, Didier; Kayser, Yves; Beckhoff, Burkhard; Lofland, Sam E.; Finkel, Peter. (2020). "In Situ Electric-Field Study of Surface Effects in Domain Engineered Pb(In1/2Nb1/2)O3-Pb(Mg1/3Nb2/3)O3-PbTiO3 Relaxor Crystals by Grazing Incidence Diffraction" *Crystals* 10, no. 9: 728. https://doi.org/10.3390/cryst10090728

This Article is brought to you for free and open access by the College of Science & Mathematics at Rowan Digital Works. It has been accepted for inclusion in Faculty Scholarship for the College of Science & Mathematics by an authorized administrator of Rowan Digital Works.

Authors

Markys G. Cain, Margo Staruch, Paul Thompson, Christopher Lucas, Didier Wermeille, Yves Kayser, Burkhard Beckhoff, Samuel Lofland, and Peter Finkel

This article is available at Rowan Digital Works: https://rdw.rowan.edu/csm_facpub/208

crystals

MDPI

Article

In Situ Electric-Field Study of Surface Effects in Domain Engineered $Pb(In_{1/2}Nb_{1/2})O_3$-$Pb(Mg_{1/3}Nb_{2/3})O_3$-$PbTiO_3$ Relaxor Crystals by Grazing Incidence Diffraction

Markys G. Cain [1,*], Margo Staruch [2], Paul Thompson [3,4], Christopher Lucas [3,4], Didier Wermeille [3,4], Yves Kayser [5], Burkhard Beckhoff [5], Sam E. Lofland [6] and Peter Finkel [2,*]

1 Electrosciences Ltd., Farnham GU9 9QT, UK
2 US Naval Research Laboratory, Washington, DC 02375, USA; margo.staruch@navy.mil
3 XMaS Beamline, European Synchrotron Radiation Facility, F-38043 Grenoble, France; pthompso@esrf.fr (P.T.); Clucas@liverpool.ac.uk (C.L.); didier.wermeille@esrf.fr (D.W.)
4 Oliver Lodge Laboratory, Department of Physics, University of Liverpool, Liverpool L69 72E, UK
5 Physikalisch-Technische Bundesanstalt, Abbestr. 2-12, 10587 Berlin, Germany; yves.kayser@ptb.de (Y.K.); burkhard.beckhoff@ptb.de (B.B.)
6 Department of Physics, Rowan University, Glassboro, NJ 08028-1701, USA; lofland@rowan.edu
* Correspondence: markys.cain@electrosciences.co.uk (M.G.C.); peter.finkel@nrl.navy.mil (P.F.)

Received: 31 July 2020; Accepted: 17 August 2020; Published: 20 August 2020

Abstract: In this work, we present a grazing incidence X-ray diffraction study of the surface of a $0.24Pb(In_{1/2}Nb_{1/2})O_3$-$Pb(Mg_{1/3}Nb_{2/3})O_3$-$PbTiO_3$ (PIN-PMN-PT) [011] poled rhombohedral single crystal. The near surface microstructure (the top several tens to hundreds of unit cells) was measured in situ under an applied electric field. The strains calculated from the change in lattice parameters have been compared to the macroscopic strain measured with a strain gauge affixed to the sample surface. The depth dependence of the electrostrain at the crystal surface was investigated as a function of temperature. The analysis revealed hidden sweet spots featuring unusually high strains that were observed as a function of depth, temperature and orientation of the lattice planes.

Keywords: piezoelectric; single crystal; sonar; characterisation; X-ray diffraction

1. Introduction

Relaxor ferroelectric single crystals are widely used as transduction materials, due to extremely high piezoelectric coefficients d_{ij} several times larger than those of commercial lead $Pb[Zr_xTi_{1-x}]O_3$ (PZT) ceramics. Recently, significant attention and resources have been put into the development of novel compositions to find better candidates based on solid solution $Pb(Mg_{1/3}Nb_{2/3})O_3$-$PbTiO_3$ (PMN-xPT) and $PbZn_{1/3}Nb_{2/3}O_3$-$PbTiO_3$ (PZN-PT), which are currently being used in medical ultrasound transducers and numerous SONAR transducer and sensors applications [1–4]. Two specific properties make these crystals ideal for applications: an extraordinarily high piezoelectric coefficient (d_{33} > 2000 pV/m) combined with an extraordinary coupling coefficient (>0.9) achieved by "domain engineering;" i.e., cutting and poling the crystals along certain planes [3,5–10]. In order to extend the linear voltage regime with higher temperature stability to greater than that of binary relaxors, the ternary single crystal system $Pb(In_{1/2}Nb_{1/2})O_3$-$Pb(Mg_{1/3}Nb_{2/3})O_3$-$PbTiO_3$ (PIN-PMN-PT) has recently been developed. This next-generation material overcomes the need for dc electrical bias to achieving high power drive, a requirement for naval projector applications.

For several decades, extensive work developing theories and experimental studies of single crystal PMN-PT and, more recently, PIN-PMN-PT has been undertaken, in order to shed light on explaining

the origins of their unique and technologically useful superior properties compared to those of their ceramic counterparts epitomized by PZT. The high strains that can be achieved in these materials are considered to be directly related to structural instabilities that exist at the morphotropic phase boundary (MPB) separating two or more crystallographic symmetries, such as the tetragonal/rhombohedral phase boundary in PZT and PMN-PT [11,12]. The situation is more complex, however, than is suggested by analysis of the MPB alone: domain engineering, polarization rotation, as well as chemical and strain gradients, all impact the electromechanical performance [13–16].

The X-ray data presented by [17] on PZN-PT relaxor systems have explored the "skin effect" previously observed in PMN-PT and PZN-PT single crystals, which refers to a difference in crystalline structure within the bulk compared to that of near the surface. For X-ray energies of 8 keV, the penetration depth is ~3 μm, which was considered to be near surface compared to those of bulk-like measurements, such as diffraction by neutrons or higher energy X-rays, for example. Neutron diffraction studies [18] have presented evidence that a skin effect exists in PMN-PT and PZN-PT, with predominantly rhombohedral phases present near the surface, and the skin effect can exist from several to even hundreds of micrometers.

The origin of these surface skin effects are not yet completely understood, and there is debate about whether the skin effect is related to an intrinsic symmetry difference between bulk and surface regions or whether the effect is related to some extrinsic mechano-polishing/grinding induced symmetry breaking of the surface [18–20]. Some early neutron diffraction studies of the skin effect for PZN single crystals identified a so-called 'X-phase' to exist at the surface and not the expected rhombohedral (F_R) phase. Additionally, a low-energy X-ray source probed the surface to some extent, and it was believed that the rhombohedral phase existed within a skin layer, caused by an imperfect poling condition at the surface of the crystal [21], somewhat contradicting their neutron results. Furthermore, neutron residual stress measurements on single crystals of PMN show the cubic lattice parameter varied with the depth normal to the crystal surface, and displayed a corresponding large surface strain [18]. That work also demonstrated how the depth dependence of strain was strongly affected by temperature, leading to incorrect phase diagrams for many of the relaxor materials. Crystal chemistry is also important and the later work of Phelan et al. [20], showed that the relaxor skin effect in PMN-xPT vanishes on the Ti-rich side of the MPB. An investigation of 33PIN-35PMN-32PT crystals [22] showed that the full width half maximum of the diffraction intensity, often an indication of inhomogeneous strain within a crystal, increased on cooling from the high-temperature cubic phase to the room-temperature bulk rhombohedral phase, which was presumed to be related to the skin effect in these relaxors. Those results indicated the presence of a surface monoclinic M_B state, which had a small but non-zero piezoelectric coefficient from X-ray diffraction measurements. After annealing the crystal in zero field, the bulk F_R phase was unpoled and showed no piezoelectric response, but the polarization vector of the surface M_B phase could be rotated easily by stress gradients, yielding non-zero piezoelectric coefficients. These results show that the skin effect, phase co-existence, and stress gradients are interrelated and impact the macroscopic properties of single crystals.

Grazing incidence X-ray diffraction is commonly used to study the crystallography near the surface as a function of depth to characterize changes in crystallography through thickness [23]. In grazing incidence techniques, the X-ray beam impinges on the surface at a very small angle with respect to the surface plane. By varying the angle of incidence α, the penetration depth of the X-ray beam in the sample can be controlled, and thus, at very shallow angles (typically below 1°), the signal originating from the surface of the sample is maximized.

Here we present the in situ electric field dependence of grazing-incidence X-ray diffraction results of a single crystal of 0.24PIN-PMN-PT, which demonstrate the non-uniformity of the effective piezoelectric coefficient near the surface. The effects temperature and depth on the field-dependent strain are measured for several different lattice planes. The analysis revealed hidden sweet spots whereby unusually high electrostrains were observed for certain depths, temperatures and orientation of the lattice planes. An important question to consider is whether the skin effect arises from (a) the

effect of residual stresses present at the surface which would depend on the nature of the atomic bonding and, hence, crystallographic orientation and surface preparation such as polishing, grinding or annealing; (b) a change in response at a free surface impacted by domain configurations; (c) a gradient in the stoichiometry (such as oxygen or cation); (d) the effect of symmetry breaking at the surface; or (e) some combination of these factors. This information is clearly very important for users of relaxor materials for MEMs or magnetoelectric composite applications, where the relevant length scale is commensurate to that of the skin effect, and would thus play a primary role in actual device performance [22].

2. Results and Discussion

2.1. Results

Figure 1 illustrates the sample geometry crystallographic orientation and poling direction of an as-prepared [011] poled PIN-PMN-PT. A Poisson ratio of 0.37 was used to match to macroscopic strain along the [001] direction to the X-ray data. Figure 2 gives the schematic of how measurements were made. Figure 3 shows the typical 'butterfly loop' bulk strain characteristics of ferroelectric materials. The coercive field is ~5.0 kV/cm, with a maximum strain of ~ 4000 microstrain (με), yielding a piezoelectric coefficient, d_{32} ~ 1327 pm/V, which closely matches that of both the manufacturer's data sheet and an independent direct piezoelectric measurement of d_{32}.

Figure 4 shows typical raw data with and without field while Figure 5 shows the typical response to the electric field E for several values of α. For the grazing incidence reflections chosen (based on 4-circle geometry and physical access to certain reciprocal lattice vectors—see Figure S2 in Supplementary Materials), the variation in d spacing is shown Figure 6 for the (010), (110), (11$\bar{1}$) and the (32$\bar{2}$) planes as a function of depth and temperature at zero field. The data show the variation in d spacing with depth of penetration of the X-rays, as expected from the literature for this material system, with a more subtle variation with temperature for all reflections except the (32$\bar{2}$). The interplanar lattice spacing changed by 0.3% for the (010) planes assuming a strain-free pseudo-cubic bulk lattice parameter of 4.04 Å. The changes for the other planes are ~0.16% for (110), ~0.1% for the (11$\bar{1}$) and ~0.02% for the (32$\bar{2}$) planes—though the actual structure for the bulk is expected to be rhombohedral for this composition at all the temperatures measured. Figure 7 shows contour plots of the field-induced change in strain as functions of temperature and depth for the various lattice planes.

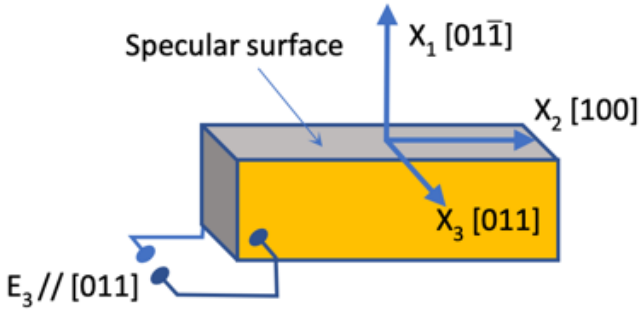

(**a**) Sample and crystallographic geometry.

Figure 1. *Cont.*

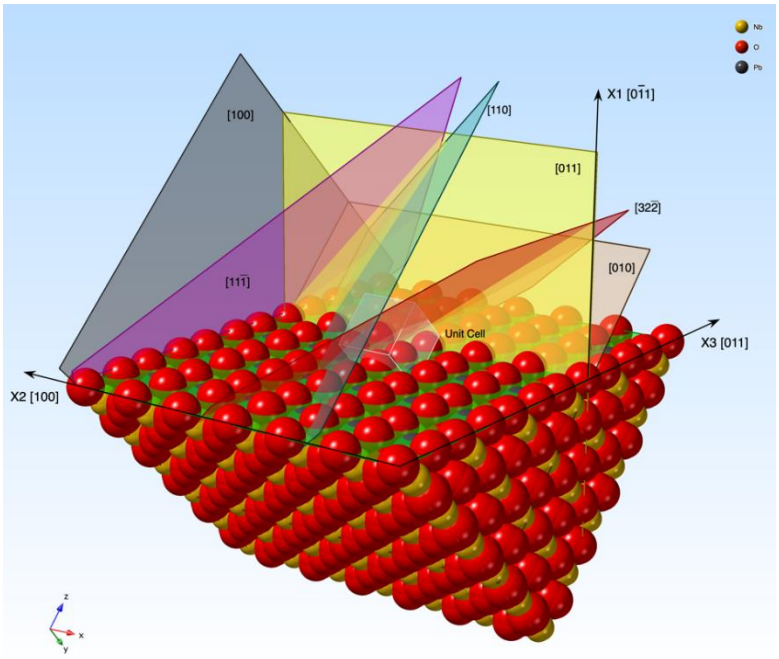

(**b**) Crystal structure schematic showing all planes explored in this study.

Figure 1. (**a**) Sample geometry and conventionally used crystallographic axes for [011] poled $Pb(In_{1/2}Nb_{1/2})O_3$-$Pb(Mg_{1/3}Nb_{2/3})O_3$-$PbTiO_3$ (PIN-PMN-PT). Note that in this work, the X-ray diffraction data utilised a pseudo cubic orientation axis. (**b**) Crystallography of X1 (01.1) specular surface of PIN-PMN-PT showing long sample X2 [100] direction, and electroded E-field direction X3 [011], with crystal planes accessible to this experiment: (010)-brown, (11$\bar{1}$)—pink, (32$\bar{2}$)—red and (110)—teal green. The crystal unit cell is also shown. (Atoms are colored as indicated and only O, Pb and Nb are shown in this cross section). CrystalMakerX v10.5.1, Begbroke, Oxfordshire, UK.

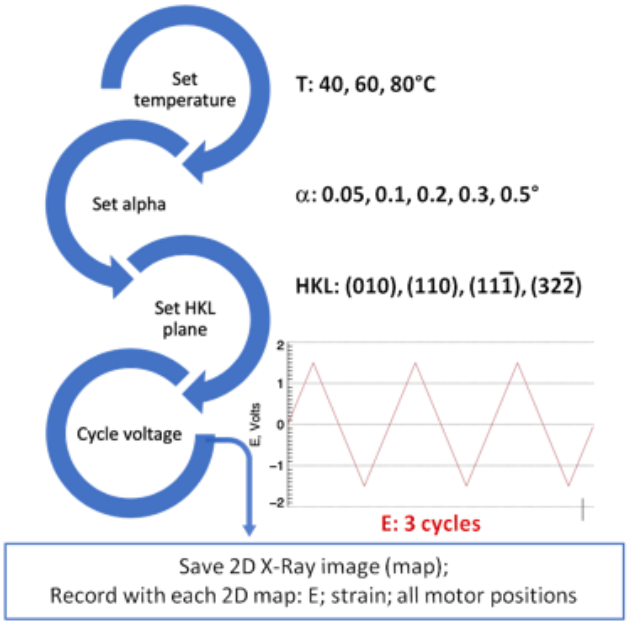

Figure 2. Schematic of the experimental methodology. The sample is clamped at approximately zero uniaxial stress into the fixture with high-voltage cabling attached as described. The bipolar voltage was cycled with a triangular waveform to yield a constant rate of voltage with time (for accurate PE loop analysis), for each set of planes at each condition of grazing incidence and temperatures.

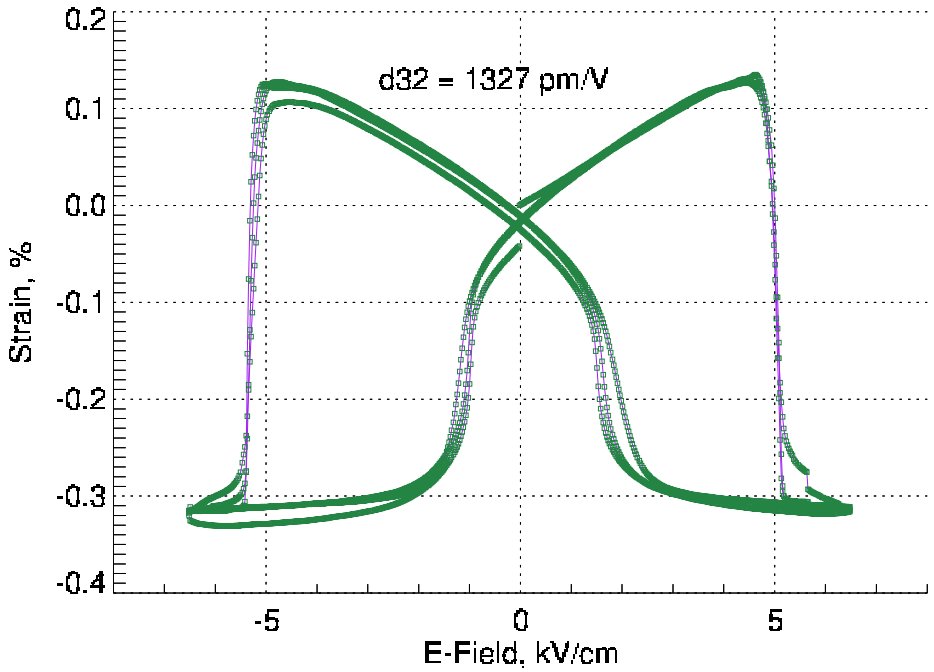

Figure 3. Macroscopic strain—field response of PIN-PMN-PT sample, showing characteristic butterfly loop response. The calculated value of d_{32} ~ 1327 pm/V. Note this measurement was carried out after the grazing incidence experiment with an increased electric field amplitude of 6.5 kV/cm in order to observe the coercive field.

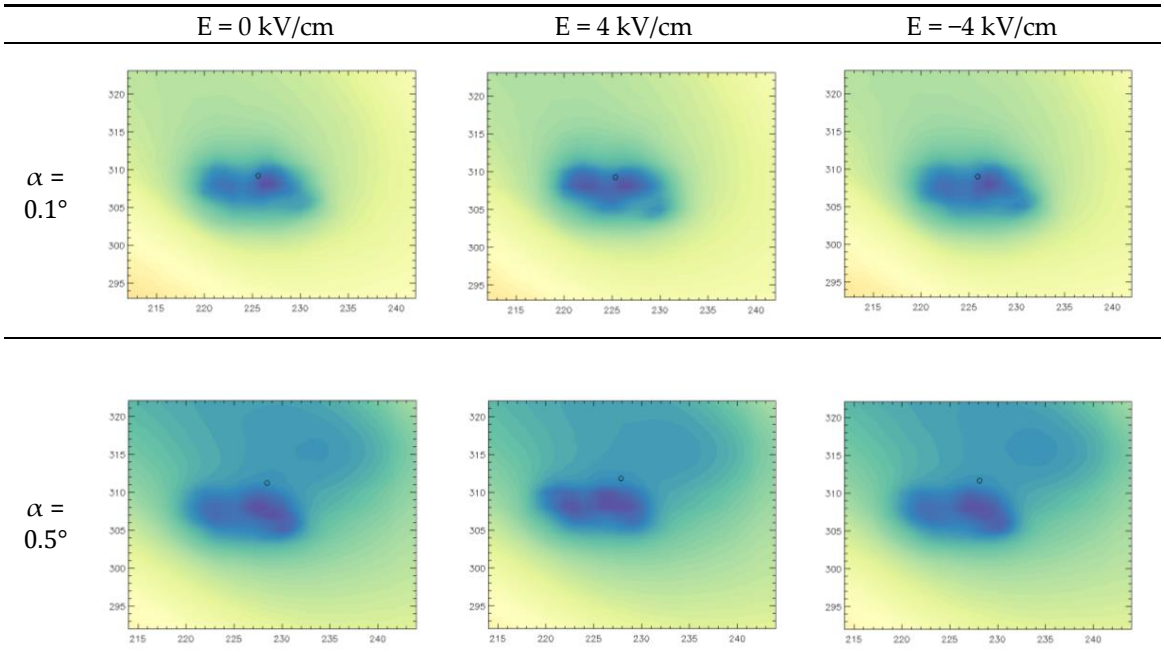

Figure 4. Raw data taken from Maxipix camera in pixel coordinates, of the (010) reflection as a function of α at 40 °C at E = 0 and ±4 kV/cm, highlighting the complex diffraction pattern obtained as a result of domain and/or twinning in the crystal. All analyses are based upon the centroid of each reflection, denoted by the small circle. As an average, the centroid should most closely resemble the macroscopic behavior.

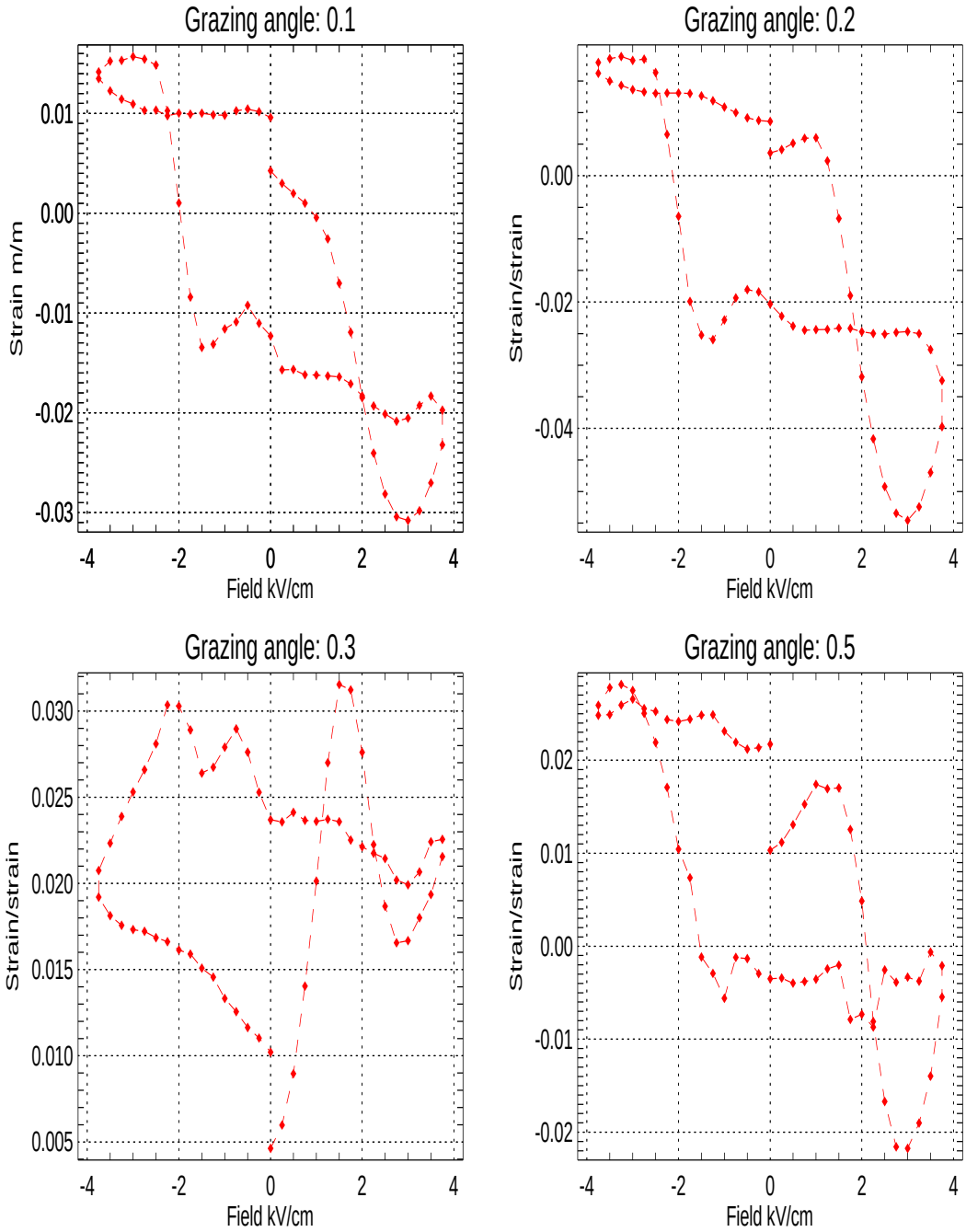

Figure 5. Electrostrain [Equation (1)] of (010) lattice plane at 40 °C as a function of E for 4 different α values. The complex depth dependent behavior shows evidence of both hysteretic ferroelectric behavior and electrostrictive quadratic field response. The two minor loops observed in the plots for positive and negative fields represents piezoelectric energy loss hysteresis as ferroelectric domains are switched in polarization with applied electric field.

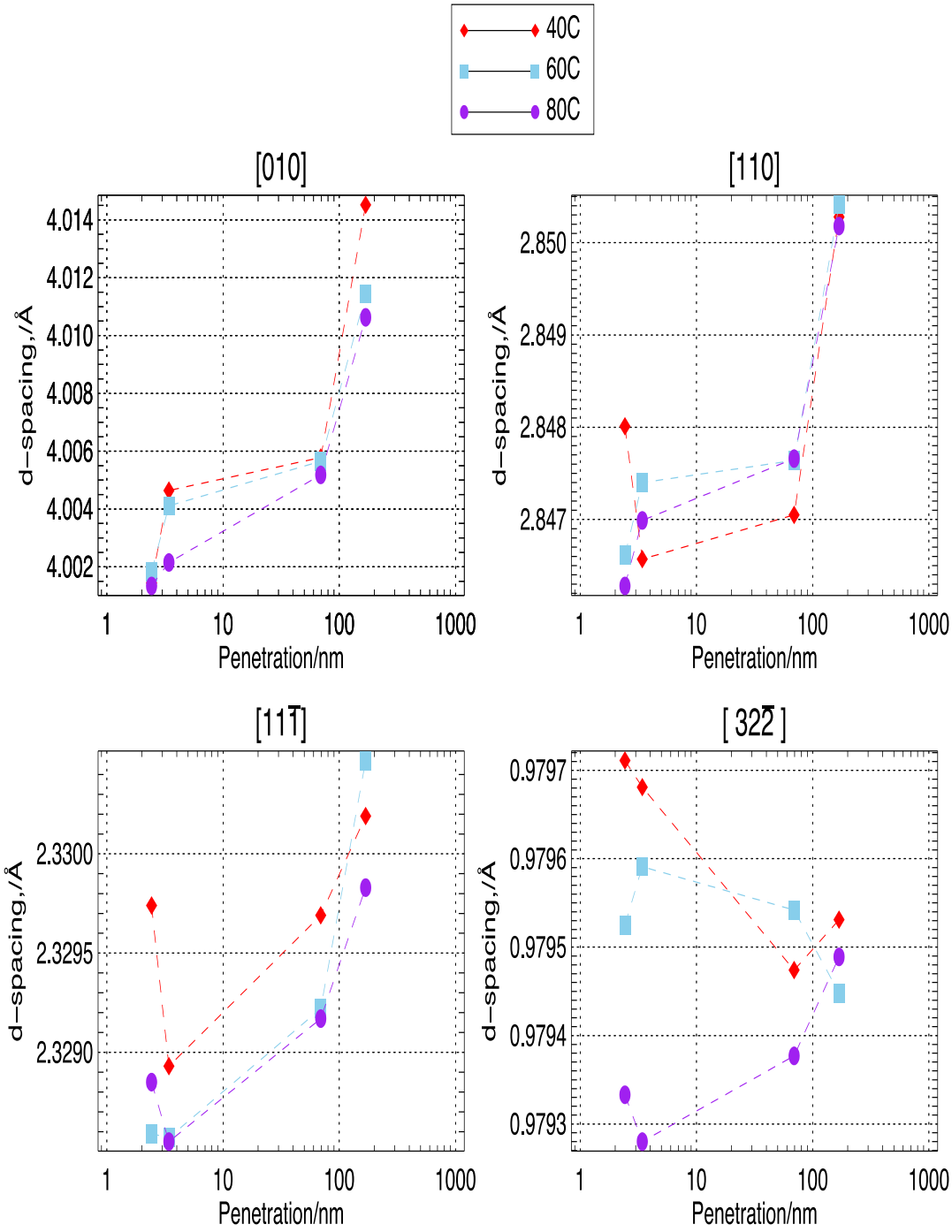

Figure 6. Lattice spacings (*d* spacing) for the grazing incidence angle reflections chosen for this study. The parameters have been calculated based on the measured *HKL* peak position, assuming pseudo cubic structure. The important features to note are the relative changes in *d* spacing for the reflections as a function of α and temperature. It is clear that at depths up to and exceeding the maximum accessed here, the *d* spacings are still changing and have not reached the 'average' bulk values, apart from the data shown for the (32$\bar{2}$) planes, which do show a degree of convergence. Each *d* spacing point has an associated error of ~ ±0.1% with an error in penetration depth of ±2 nm [Supplementary Materials, Equation (2)].

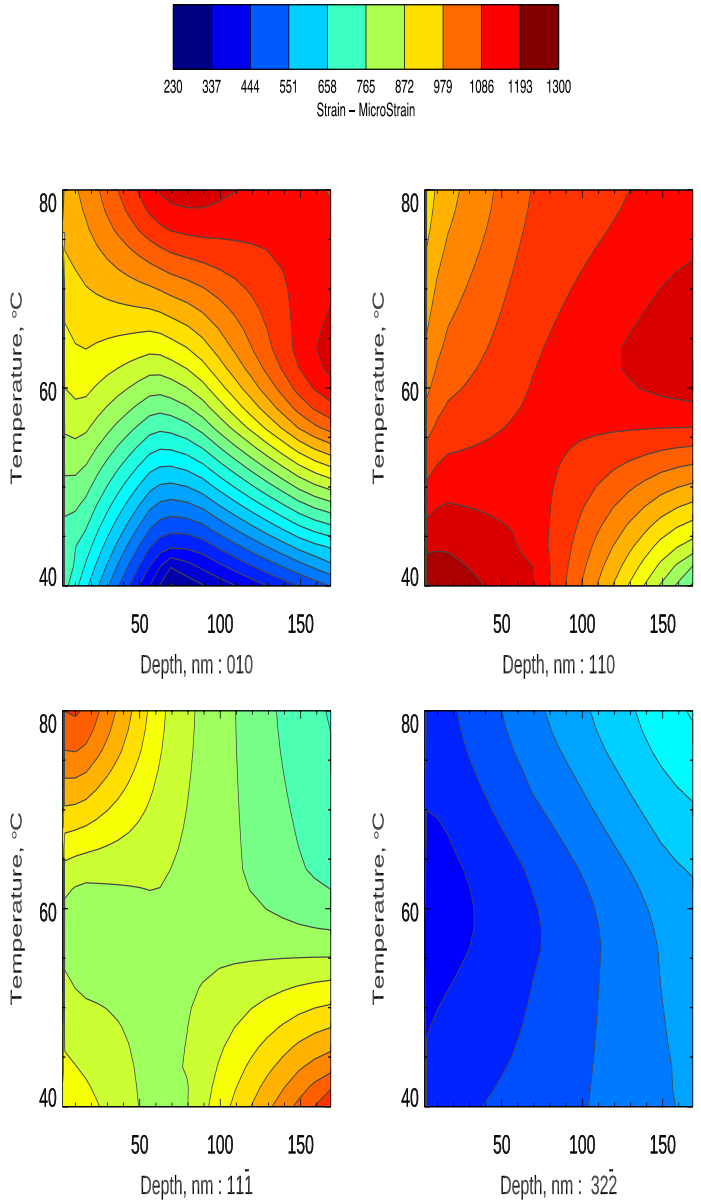

Figure 7. Contour maps of the electrostrain [Equation (1)] for different lattice planes as a function of temperature and depth from the surface of the sample (~2 nm) into its bulk. The contours have been linearly interpolated from the data taken at three specific temperatures and five values of α. These specific temperatures were chosen as representing a range commonly used in real life applications for this class of material.

2.2. Discussion

The present results on polished single crystals of 24%PIN-PMN-PT indicate that strain gradients persist down to hundreds of nm. Reduced dielectric and piezoelectric properties are often observed with decreasing sample size and generally correlate to surface damage as a result of lapping and polishing although the thickness effect is not solely due to mechanical-chemical polishing [24]. For instance, results from relaxor PMN-PT ceramics and crystals showed that the dielectric and piezoelectric properties were correlated with their domain size [24]. Domain sizes for PIN-PMN-PT single crystals and thin films have been shown to be dependent on large variety of factors and examples ranging from tens to a few hundreds of nm have been recorded [24–29], although tens of nm is more typical.

The current studies probe down to the top few hundred nm, depths larger than typical domain sizes. Thus, the measured strain response then should mostly exclude the extrinsic domain reorientation contribution for the reflections measured at larger α values. The macroscopic field-strain response of the relaxor class of material arises from the intrinsic electrostrictive coefficient and its piezoelectric response. The two responses are often reported as simply the piezo response, but the observation can be differentiated via the quadratic response to field observed for electrostriction compared to linear dependence of polarization with field for the piezo effect. In relaxor ferroelectrics both physical processes are generally responsible for their actual response [26,30]. The field dependence of the strain response from several of the measured lattice planes (Figure 5) displays a mix of both behaviors and is more complex than the bulk behavior (Figure 3). A double loop hysteretic response is observed in all plots in positive and negative going voltage excursions indicating ferroelectric behavior superimposed on a linear response indicative of an electrostrictive response. Note that at the larger depths (lower panel, Figure 4), it is clear that local structure is distinct from that of the surface.

An additional factor that affects the strain response from different planes is based on the degree to which those planes are affected by domain reorientation under an applied electric field (Figure 4, upper panel). This particular sample was poled along the [011] direction with the local polarization aligned with the cubic [111] directions, which may rotate under electric and stress fields, to reduce the domain density (from multi domain to single domain for example—see [12]). In the ideal engineered crystal of this type, there are two equivalent [111] polarization directions within the crystal. In the present case, there is zero applied stress with only thermal and electrical excitation (stress-induced phase changes are the subject of a future paper, though elements are reported here [31]). Our data identifies lattice reflections near the free surface (<200 nm) that exhibit a higher degree of strain compared to others. While there is a weak depth dependence of $(33\bar{2})$ planes, the other showed significant changes with depth with (010) > (110) > $(11\bar{1})$ at 40 °C.

The strain dependence on temperature also presents some interesting features: for the (010) and (110) reflections, we note higher temperatures generally feature larger strains, which supports the thermodynamic view linking increased domain mobility with increasing temperature [6]. An interesting anomaly rests with the $(11\bar{1})$ reflection data, however, with a peak in strain at high temperature/shallow depth and low temperature/high depth (Figure 7). The absolute values of strain are perhaps less important than the relative changes for any given reflection since the behavior is determined by the full tensor response of the crystal. For example, planes aligned parallel to the specular surface representing the d_{31} coefficient and those planes parallel to the long axis of the sample [100] direction representing the d_{32} coefficient have an inherently different response. In these experiments, none of the grazing incidence planes are aligned to those primary directions, so a direct piezoelectric coefficient calculation was not possible. However, the specular reflection $(01\bar{1})$ corresponds with the out of plane d_{31} coefficient, which, coupled to the strain gauge data, means a value of the piezoelectric d_{32} coefficient can be calculated from the appropriate Poisson ratio. The strain associated with the (110) planes closely matches that measured with the strain gauge data. The (110) planes are inclined at an angle of 60° to the electric field direction ([011] X3) and 30° to the [100] X2 axis, and so the resolved strain within that set of planes with respect to the sample surface is expected to most closely match d_{32} of the crystal, which is ~ (1600 με)/(cos60° sin60°) ~ 3700 με, close to the value of ~ 4000 με, measured by the strain gauge along X1 direction. We note that the analysis here is highly simplified and resolving strains into different directions from known lattice parameter changes is non-trivial, but this serves as a good first approximation.

3. Experimental Section

A rectangular bar of 0.24 PIM-PMN-PT with dimensions $4 \times 4 \times 12$ mm^3 was supplied by CTS Corporation, USA. For sample details see Table S1 in Supplementary Information. The specular surface in the chosen coordinate system of the sample was X1 $[01\bar{1}]$ oriented, with the long direction of the sample along the X2 [100] axis and $\boldsymbol{E}$ along the X3 [011] axis (Supplementary Information

Figure S1).The macroscopic strain was recorded along [100] with a strain gauge attached to the sample surface (Supplementary Information Figure S3).

Sample electrodes were made by depositing evaporated gold onto the $[1\bar{1}0]$ faces (perpendicular to the sample surface normal). See Figure 1, Figures S1 and S2 for more details of sample orientation and GIXRD geometry. After the surfaces are ground and polished to $\sim\frac{1}{4}$ µm, the sample was mounted with low melting temperature wax onto an insulating substrate. High-voltage wiring was affixed to the sample jig and connected to a TREK 610E HV amplifier. Ferroelectric current as a function of applied voltage was measured with a virtual earth current amplifier, and the charge was then calculated through numerical integration [32]. Details are provided in reference [33], and shown in Figure S3.

The diffracted intensity was recorded with a PILATUS3 X 300K imaging camera from Dectris (Baden-Daettwil, Switzerland). The applied voltage, ferroelectric current and X-ray intensity were all measured simultaneously and recorded with a data acquisition system based on the ESRF-designed MUSST card. The card can simultaneously record X-ray intensities and analogue voltages up to 24 bit resolution with a sampling rate of 40 kHz [33]. The full in situ capabilities at the XMaS beamline, ESRF, for characterizing ferroelectrics, developed by Electrosciences and the University of Liverpool, include electric field, temperature, frequency, magnetic field and stress. The experimental methodology is graphically represented in Figure 2.

The penetration depth of the X-rays normal to the surface is proportional to the sin α for angles greater than the critical angle, the angle of total external reflection, which is related to the wavelength-dependent refractive index of the sample (see Figures S2 and S6 in Supplementary Information). The X-ray energy was 12.4 keV (wavelength = 1 Å) and measurements were done with $0.05° < \alpha < 0.5°$, corresponding to a penetration depth ranging between 2 and 200 nm, which is an order of magnitude lower than that of previously published data on similar materials systems. More details can be found in Supplementary Information.

The scattering geometry only permitted a selection of accessible reflections as defined in Figure 1. A crystal representation of the surface of the sample is shown in Figure 1b, with the [110] specular normal shown as the top surface atom cut, and the indices of the planes used in this study also labelled. The camera pixel coordinate frame was translated to *HKL* pseudocubic Miller indices by a program written in Python which extensively uses various PyMca (v5.4.2) modules [34]. Additional data analysis and visualization were performed on the *HKL* indexed images, with code written in IDL V 8.7.2 (Harris Geospatial Solutions, Inc., Broomfield, CO, USA) although data were interpolated only once within the *HKL* conversion process. Detailed analysis of all reflections and at all values for α and temperature was carried out following the approach outlined in the Supplementary Information. The 3D *HKL* volume data sets were then analysed to calculate the d spacing d_E^{HKL} at $E = 4$ kV/cm for each value of temperature, *HKL* and α. These data were then plotted as the electrostrain δ relative to the d spacing at $E = 0$ (d_0^{HKL}) for each α value. That is

$$\delta = \frac{d_E^{HKL} - d_0^{HKL}}{d_0^{HKL}} \quad (1)$$

as plotted in Figures 5 and 7.

4. Conclusions

The work has probed the strain associated with a variety of reflections taken in grazing incidence geometry for a single crystal of [011] poled rhombohedral PIN-PMN-PT relaxor ferroelectric as a function of electric field and temperature. The strain calculated from changes in lattice parameters have been compared to the macroscopic strain measured with a strain gauge affixed to the sample surface. A measurable depth dependence of lattice parameter and calculation of in operando strain identifies those planes which have a higher sensitivity to field, indicating an opportunity for optimizing strain interfaces in, for example, energy harvesting magnetoelectric composites. Application of mechanical

stress affects the crystallographic strain dramatically [12,31], which would have significant impact on the strain transfer optimization across an interface in magnetoelectric composites, for example, details of which will be reported in a future publication. The origin of this observed skin effect due to (a) residual stress, (b) domain configuration, (c) stoichiometry or (d) symmetry breaking is yet to be confirmed, but is likely to be a combination of all such mechanisms. Finally, for future studies, the methodologies for in operando study of electric-field-driven structural phase changes in these materials by synchrotron X-ray diffraction have been established for grazing incidence geometry, and work will focus on development of machine learning tools to accurately follow the diffraction peaks as a function of field temperature, and depth, to augment and accelerate experimental data analysis and phase identification, stability and link to the material's functional performance.

Supplementary Materials: The following are available online at http://www.mdpi.com/2073-4352/10/9/728/s1, Table S1: Composition and some properties of samples measured; Figure S1: Two coordinate systems used in the study. specular face in right hand diagram; Figure S2: Grazing Incidence X-Ray diffraction for PIN-PMN-PT, Figure S3: Attachment of the strain gauge (RS Pro 2.5mm gauges 120 Ω 632-146) to the single crystal using cyanoacrylate adhesive, leaving sufficient space for the X-Ray beam off this specular surface; Figure S4: Calculation of the penetration depth of X-Rays.

Author Contributions: Authors contributed: the experiment was performed by M.G.C., P.T., Y.K., B.B. Manuscript was written by M.G.C., S.E.L., P.F., C.L. and M.S. Data analysis was performed by M.G.C. with software developed by M.G.C. and D.W. All authors have read and agreed to the published version of the manuscript.

Funding: The authors would like to acknowledge funding from the Office of Naval Research under the U.S. Naval Research Laboratory's Basic Research Program, and Office of Naval Research Global, ONRG—NICOP Project Number: N62909-18-1-2008 Electrosciences Ltd. Parts of this research work was carried in the framework of the ADVENT project (Grant Number: 16ENG06 ADVENT) which is supported by the European Metrology Programme for Innovation and Research (EMPIR). The EMPIR initiative is co-funded by the European's Horizon 2020 research and innovation programme and the EMPIR Participating States. XMaS is a UK National Research Facility funded by EPSRC.

Conflicts of Interest: The authors declare no conflict of interest.

References

1. Park, S.E.E.; Hackenberger, W. High performance single crystal piezoelectrics: Applications and issues. *Curr. Opin. Solid State Mater. Sci.* **2002**, *6*, 11–18. [CrossRef]
2. Zhang, S.; Shrout, T. Relaxor-PT single crystals: Observations and developments. *IEEE Trans. Ultrason. Ferroelectr. Freq. Contr.* **2010**, *57*, 2138–2146. [CrossRef] [PubMed]
3. Sun, E.; Cao, W. Relaxor-based ferroelectric single crystals: Growth, domain engineering, characterization and applications. *J. Prog. Mater. Sci.* **2014**, *65*, 124–210. [CrossRef] [PubMed]
4. Hosono, Y.; Yamashita, Y. Piezoelectric ceramics and single crystals for ultrasonic medical transducers. *J. Electroceram* **2006**, *17*, 577–583. [CrossRef]
5. Li, F.; Zhang, S.; Luo, J.; Geng, X.; Xu, Z.; Shrout, T.R. [111]-oriented PIN-PMN-PT crystals with ultrahigh dielectric permittivity and high frequency constant for high-frequency transducer applications. *J. Appl. Phys.* **2016**, *120*, 074105. [CrossRef]
6. Qiao, H.; He, C.; Wang, Z.; Li, X.; Liu, Y.; Tailor, H.; Long, X. Orientation-dependent electrical property and domain configuration of Mn-doped Pb(In 0.5Nb 0.5)O 3-PbTiO 3single crystal. *J. Am. Ceram. Soc.* **2018**, *102*, 79–84. [CrossRef]
7. Li, F.; Zhang, S.; Xu, Z.; Wei, X.; Luo, J.; Shrout, T.R. Investigation of Electromechanical Properties and Related Temperature Characteristics in Domain-Engineered Tetragonal Pb(In1/2Nb1/2)O3-Pb(Mg1/3Nb2/3)O3-PbTiO3 Crystals. *J. Am. Ceram. Soc.* **2010**, *93*, 2731–2734. [CrossRef]
8. Bell, A.J. Ferroelectrics: The role of ceramic science and engineering. *J. Eur. Ceram. Soc.* **2008**, *28*, 1307–1317. [CrossRef]
9. Damjanovic, D.; Brem, F.; Setter, N. Crystal orientation dependence of the piezoelectric d[sub 33] coefficient in tetragonal BaTiO[sub 3] as a function of temperature. *Appl. Phys. Lett.* **2002**, *80*, 652. [CrossRef]
10. Damjanovic, D. Contributions to the Piezoelectric Effect in Ferroelectric Single Crystals and Ceramics. *J. Am. Ceram. Soc.* **2005**, *88*, 2663–2676. [CrossRef]

11. Damjanovic, D. A morphotropic phase boundary system based on polarization rotation and polarization extension. *Appl. Phys. Lett.* **2010**, *97*, 062906. [CrossRef]
12. Finkel, P.; Staruch, M.; Amin, A.; Ahart, M.; Lofland, S.E. Simultaneous Stress and Field Control of Sustainable Switching of Ferroelectric Phases. *Sci. Rep.* **2015**. [CrossRef] [PubMed]
13. Nan, C.-W.; Bichurin, M.I.; Dong, S.; Viehland, D.; Srinivasan, G. Multiferroic magnetoelectric composites: Historical perspective, status, and future directions. *J. Appl. Phys.* **2008**, *103*, 031101. [CrossRef]
14. Noheda, B.; Cox, D.; Shirane, G.; Gonzalo, J.; Cross, L.; Park, S. A monoclinic ferroelectric phase in the Pb (ZrTi) O solid solution. *Appl. Phys. Lett.* **1999**, *74*, 2059. [CrossRef]
15. Fu, H.; Cohen, R. Polarization rotation mechanism for ultrahigh electromechanical response in single-crystal piezoelectrics. *Nature* **2000**, *403*, 281–283. [CrossRef]
16. Park, S.-E.; Shrout, T.R. Ultrahigh strain and piezoelectric behavior in relaxor based ferroelectric single crystals. *J. Appl. Phys.* **1997**, *82*, 1804. [CrossRef]
17. Wang, Y.; Wang, D.; Yuan, G.; Ma, H.; Xu, F.; Li, J.; Viehland, D.; Gehring, P.M. Fragile morphotropic phase boundary and phase stability in the near-surface region of the relaxor ferroelectric (1-x) Pb (Z n1 /3N b2 /3) O3-x PbTi O3: [001] field-cooled phase diagrams. *Phys. Rev. B* **2016**, *94*, 174103. [CrossRef]
18. Xu, G.; Gehring, P.M.; Stock, C.; Conlon, K. The anomalous skin effect in single crystal relaxor ferroelectric PZN-x PT and PMN-x PT. *Phase Transit.* **2006**, *79*, 135–152. [CrossRef]
19. Cowley, R.A.; Gvasaliya, S.N.; Lushnikov, S.G.; Roessli, B.; Rotaru, G.M. Relaxing with relaxors: A review of relaxor ferroelectrics. *Adv. Phys.* **2011**, *60*, 229–327.
20. Phelan, D.; Rodriguez, E.E.; Gao, J.; Bing, Y.; Ye, Z.G.; Huang, Q.; Wen, J.; Xu, G.; Stock, C.; Matsuura, M.; et al. Phase diagram of the relaxor ferroelectric (1-x) Pb(Mg1/3Nb2/3)O3+xPbTiO3 revisited: A neutron powder diffraction study of the relaxor skin effect. *Phase Transit.* **2015**, *88*, 283–305. [CrossRef]
21. Xu, G.; Zhong, Z.; Bing, Y.; Ye, Z.G.; Stock, C.; Shirane, G. Ground state of the relaxor ferroelectric Pb(Zn1/3Nb2/3)O3. *Phys. Rev. B Condens. Matter* **2003**, *67*, 1804–1805. [CrossRef]
22. Wang, Y.; Yuan, G.; Luo, H.; Li, J.; Viehland, D. Phase Transition in the Near-Surface Region of Ternary Pb(In1/2Nb1/2)O3−Pb(Mg1/3Nb2/3)O3−PbTiO3Relaxor Ferroelectric Crystals. *Phys. Rev. Appl.* **2017**, *8*, 034032. [CrossRef]
23. Feidenhans'l, R. Surface structure determination by X-ray diffraction. *Surf. Sci. Rep.* **1989**, *10*, 105–188. [CrossRef]
24. Lee, H.J.; Zhang, S.; Luo, J.; Li, F.; Shrout, T.R. Thickness-Dependent Properties of Relaxor-PbTiO3 Ferroelectrics for Ultrasonic Transducers. *Adv. Funct. Mater.* **2010**, *20*, 3154–3162. [CrossRef] [PubMed]
25. Wang, H.; Zeng, K. Domain structure, local surface potential distribution and relaxation of Pb(Zn1/3Nb2/3)O3-9%PbTiO3 (PZN-9%PT) single crystals. *J. Mater.* **2016**, *2*, 309–315. [CrossRef]
26. Qi, X.; Zhao, Y.; Sun, E.; Du, J.; Li, K.; Sun, Y.; Yang, B.; Zhang, R.; Cao, W. Large electrostrictive effect and high energy storage performance of Pr^{3+}-doped PIN-PMN-PT multifunctional ceramics in the ergodic relaxor phase. *J. Eur. Ceram. Soc.* **2019**, *39*, 4060–4069. [CrossRef]
27. Vlasov, E.O.; Chezganov, D.S.; Gimadeeva, L.V.; Ushakov, A.D.; Hu, Q.; Wei, X.; Shur, V.Y. Domain structure imaging in PMN-PT crystals using channelling-contrast backscattered electron microscopy. *IOP Conf. Ser. Mater. Sci. Eng.* **2018**, *443*, 012038. [CrossRef]
28. Herdier, R.; Leclerc, G.; Poullain, G.; Bouregba, R.; Remiens, E.D.; Dogheche, E. Investigation of Piezoelectric and Electrostrictive Properties of (Pb 1-3 y/2,La y) (Zr x,Ti 1-x)O 3Ferroelectric Thin Films Using a Doppler Laser Vibrometer. *Ferroelectrics* **2010**, *362*, 145–151. [CrossRef]
29. He, W.; Li, Q.; Xi, X.; Yan, Q. High temperature-insensitive ferro-/piezoelectric properties and nanodomain structures of Pb(In 1/2Nb 1/2)O 3-PbZrO 3-Pb(Mg 1/3Nb 2/3)O 3-PbTiO 3relaxor single crystals. *J. Am. Ceram. Soc.* **2017**, *101*, 1236–1244. [CrossRef]
30. Detalle, M.; Herdier, R.; Wang, G.S.; Remiens, D.; Roussel, P.; Fribourg-Blanc, E. Electrostrictive and Piezoelectric Behavior of PMN-PT Thin Films. *Ferroelectrics* **2007**, *351*, 15–24. [CrossRef]
31. Patterson, E.A.; Staruch, M.; Matis, B.R.; Young, S.; Lofland, S.E.; Antonelli, L.; Blackmon, F.; Damjanovic, D.; Cain, M.G.; Thompson, P.B.J.; et al. Dynamic piezoelectric response of relaxor single crystal under electrically driven inter-ferroelectric phase transformations. *Appl. Phys. Lett.* **2020**, *116*, 222903. [CrossRef]
32. Cain, M.G. Springer series in measurement science and technology. In *Characterisation of Ferroelectric Bulk Materials and Thin Films*; Springer: Berlin, Germany, 2014.

33. Vecchini, C.; Thompson, P.; Stewart, M.; Muniz-Piniella, A.; McMitchell, S.R.C.; Wooldridge, J.; Lepadatu, S.; Bouchenoire, L.; Brown, S.; Wermeille, D.; et al. Simultaneous dynamic electrical and structural measurements of functional materials. *Rev. Sci. Instrum.* **2015**, *86*, 103901. [CrossRef] [PubMed]
34. Solé, V.A.; Papillon, E.; Cotte, M.; Walter, P.; Susini, J. A multiplatform code for the analysis of energy-dispersive X-ray fluorescence spectra. *Spectrochim. Acta Part. B At. Spectrosc.* **2007**, *62*, 63–68. [CrossRef]

© 2020 by the authors. Licensee MDPI, Basel, Switzerland. This article is an open access article distributed under the terms and conditions of the Creative Commons Attribution (CC BY) license (http://creativecommons.org/licenses/by/4.0/).